THE JOURNAL OF BIOLOGICAL CHEMISTRY
Vol. 280, No. 18, Issue of May 6, pp. 18202–18210, 2005

Printed in U.S.A.

Crystal Structures of the RNA-dependent RNA Polymerase Genotype 2a of Hepatitis C Virus Reveal Two Conformations and Suggest Mechanisms of Inhibition by Non-nucleoside Inhibitors*

Received for publication, November 29, 2004, and in revised form, February 23, 2005
Published, JBC Papers in Press, March 2, 2005, DOI 10.1074/jbc.M413410200

Bichitra K. Biswal‡, Maia M. Cherney‡, Meitian Wang‡, Laval Chan§, Constantin G. Yannopoulos§, Darius Bilimoria§, Olivier Nicolas§, Jean Bedard§, and Michael N. G. James‡¶

From the ‡Canadian Institutes of Health Research Group in Protein Structure and Function, Department of Biochemistry, University of Alberta, Edmonton, Alberta T6G 2H7, Canada and §ViroChem Pharma Incorporated, Laval, Quebec H7V 4A7, Canada

Crystal structures of the RNA-dependent RNA polymerase genotype 2a of hepatitis C virus (HCV) from two crystal forms have been determined. Similar to the three-dimensional structures of HCV polymerase genotype 1b and other known polymerases, the structures of the HCV polymerase genotype 2a in both crystal forms can be depicted in the classical right-hand arrangement with fingers, palm, and thumb domains. The main structural differences between the molecules in the two crystal forms lie at the interface of the fingers and thumb domains. The relative orientation of the thumb domain with respect to the fingers and palm domains and the β-flap region is altered. Structural analysis reveals that the NS5B polymerase in crystal form I adopts a "closed" conformation that is believed to be the active form, whereas NS5B in crystal form II adopts an "open" conformation and is thus in the inactive form. In addition, we have determined the structures of two NS5B polymerase/non-nucleoside inhibitor complexes. Both inhibitors bind at a common binding site, which is nearly 35 Å away from the polymerase active site and is located in the thumb domain. The binding pocket is predominantly hydrophobic in nature, and the enzyme inhibitor complexes are stabilized by hydrogen bonding and van der Waals interactions. Inhibitors can only be soaked in crystal form I and not in form II; examination of the enzyme-inhibitor complex reveals that the enzyme has undergone a dramatic conformational change from the form I (active) complex to the form II (inactive).

Hepatitis C virus (HCV)[1] is a debilitating human pathogen affecting an estimated 3% of the world's population (1). The virus establishes chronic infection in the majority of the cases, eventually leading to the development of liver diseases such as cirrhosis and hepatocellular carcinoma in almost 15–20% of those infected. Although a great deal of research has been focused on the development of anti-HCV agents, to date no vaccine is available and there is no effective therapy for all genotypes of HCV. The current therapies (a combination of polyethylene glycol-treated α-interferon and ribavirin) are associated with limited efficacy and severe adverse side effects. Therefore, the development of HCV-specific antiviral agents is needed urgently to alleviate this serious health problem.

HCV is a positive single-stranded-RNA virus and a member of the Flaviviridae family (2). Six major genotypes and 11 subtypes of HCV are known. The viral genome is comprised of a single open reading frame that codes a polyprotein of ~3000 amino acids (1). The polyprotein is subsequently processed into individual components by host and viral-encoded peptidases. The polyprotein consists of three structural proteins (C, E1, and E2) and six non-structural proteins (NS2, NS3, NS4A, NS4B, NS5A, and NS5B) (3–5). Among these, NS5B polymerase and the NS3 peptidase-helicase are the key enzymes involved in the genome replication and polyprotein processing of HCV. Therefore, these enzymes are potential drug targets, emphasizing the need for detailed studies of these enzymes in HCV.

NS5B has been characterized as an RNA-dependent RNA polymerase (RdRP) based on *in vitro* experiments (6, 7). Several crystal structures of NS5B HCV polymerase (HCV-BK, genotype 1b) in several crystalline forms have been determined. The structure resembles a right hand with fingers, palm, and thumb domains (8–10). More importantly, HCV polymerase has a fully encircled active site that is unique compared with other polymerases. The structure of HCV polymerase in complex with ribonucleotides has been analyzed (11). Recently substrate complexes of HCV RNA polymerase (HC-J4), describing nucleotide import and *de novo* initiation, have revealed that the polymerase does not undergo marked structural changes upon nucleotide binding (12). Structures of the RNA-dependent RNA polymerases from polio, bacteriophage Φ6, and rabbit hemorrhagic disease viruses are also known (13–15). Structures of unliganded and ternary complexes of the polymerase from human immunodeficiency virus type 1 reverse transcriptase (HIV1-RT), which is both an RNA- and a DNA-dependent DNA polymerase, have been determined (16, 17). The thumb domain of the HIV1-RT polymerase moves ~20° upon binding the template, primer nucleic acid.

Despite the low sequence homology among polymerases, conserved domain organization persists among RNA-dependent RNA polymerases, DNA-dependent DNA polymerases, DNA-

* This work was supported in part by funding from the Alberta Heritage Foundation for Medical Research for the purchase of area detector facilities and Canadian Institutes of Health Research for operating expenses. The costs of publication of this article were defrayed in part by the payment of page charges. This article must therefore be hereby marked "*advertisement*" in accordance with 18 U.S.C. Section 1734 solely to indicate this fact.

The atomic coordinates and structure factors (codes 1YUY, 1YV2, 1YVZ, and 1YVX) have been deposited in the Protein Data Bank, Research Collaboratory for Structural Bioinformatics, Rutgers University, New Brunswick, NJ (http://www.rcsb.org/).

¶ Canada Research Chair in Protein Structure and Function and to whom correspondence should be addressed. Tel.: 780-492-4550; Fax: 780-492-0886; E-mail: Michael.james@ualberta.ca.

[1] The abbreviation used is: HCV, hepatitis C virus.

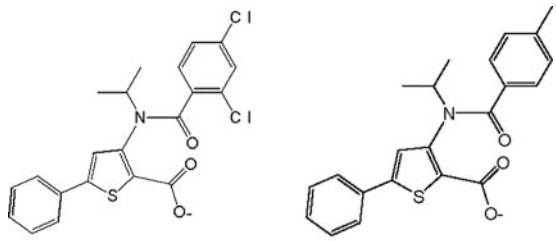

FIG. 1. **Chemical structures of non-nucleoside inhibitors A and B.**

dependent RNA polymerases, and RNA-dependent DNA polymerases. For a complete understanding of structure-function relationships, it is imperative to have structural knowledge of the HCV polymerases from all of the available genotypes. Here, we report in the first part of the paper the x-ray crystal structures of the HCV polymerase genotype 2a from two different crystal forms.

Both nucleoside and non-nucleoside inhibitors of HCV NS5B polymerase have been discovered recently (18, 19), and we have recently reported on the crystal structures of HCV polymerase genotype 1b/inhibitor complexes (20). As part of ongoing efforts to study protein/inhibitor complexes for the development of antiviral drugs, we have determined the structure of HCV polymerase genotype 2a complexed with two thiophene 2-carboxylic acid non-nucleoside inhibitors (Fig. 1). These inhibitors were synthesized as part of ongoing structure-activity relationship optimization efforts that have been described elsewhere (21–23). The details of the inhibitor binding site, protein-inhibitor interactions, and plausible mechanisms of inhibition will be discussed in the second part of the paper. The HCV polymerase genotype 2a used in the present study contains a C-terminal deletion of 21 amino acid residues (Δ21) and an N-terminal hexahistidine tag.

MATERIALS AND METHODS

Purification and Biochemical Studies—For crystallographic studies and measurement of the inhibitory effects of compounds, a soluble C-terminal truncated form of the polymerase 2a enzyme was obtained by the following approach. A full-length synthetic gene was produced initially by a PCR-mediated gene assembly based on the procedure described by Stemmer *et al.* (24). HCV polymerase 2a full-length sequences were identified from the NCBI data bank, and a consensus sequence based on codon usage in bacteria was produced. From this consensus sequence, a series of overlapping oligonucleotides (Invitrogen) spanning the complete gene were synthesized. The gene assembly procedure was performed by fusion PCR in two steps. Briefly, the first step involved the production of four sub-fragments of the gene, each containing overlapping sequences for the second gene assembly step. Each of the four reactions underwent one round of annealing/extension (40 cycles of 94 °C 20 s, 51 °C for 20 s, and 72 °C for 45 s) using Vent polymerase (New England Biolabs). Following the annealing/extension of the primers, the product was diluted 100-fold, and the outer primers of each fragment were added for a round of amplification (40 cycles of 94 °C for 30 s, 62 °C for 30 s, and 72 °C for 90 s). For the second step, the product of each reaction was then diluted 25-fold and annealed together (40 cycles at 94 °C for 20 s, 62 °C for 20 s, and 72 °C for 45 s). A second round of PCR (40 cycles at 94 °C for 30 s, 62 °C for 30 s, and 72 °C for 120 s) was performed by diluting the annealed fragments 100-fold and using the outer primers to create the complete full-length gene. Then, the final PCR product was cloned and used as a PCR template for the production of the HCV polymerase 2a Δ21 using a 5′-primer containing a His tag and a 3′-primer 63 bases upstream from the stop codon. This PCR product was cloned into a pET-21b vector (Novagen Inc., Madison, WI), and its sequence was confirmed by DNA sequencing and then expressed in *Escherichia coli* BL21 (DE3). Soluble polymerase was subsequently obtained as described previously (24). Briefly, the polymerase was initially purified using Hi-Trap nickel-nitrilotriacetic affinity chromatography with a 10–500 mM imidazole gradient. The polymerase fractions were pooled, and the imidazole was removed using PD10 desalting columns (Amersham Biosciences). Further purification of the polymerase was performed by passing the nickel-nitrilotriacetic fractions through a Hi-Trap Mono S cation exchange column. Positive fractions were exchanged into a buffer containing 10 mM Tris, pH 7.5, 10% glycerol, 5 mM dithiothreitol, and 600 mM NaCl, and glycerol was added to a final concentration of 40% for storage at −80 °C and for subsequent activity and kinetic assays. Protein for crystal structure studies was concentrated using an Ultra-15 centrifugal filter unit (Millipore) to ~10 mg/ml and stored at 4 °C.

In Vitro NS5B Assay—The inhibitory effects of compounds on HCV NS5B genotype 2a polymerization activity were measured by evaluating the amount of radiolabeled UTP incorporated by the enzyme on a homopolymeric RNA template/primer (24, 25). The 50% inhibitory concentrations (IC_{50}) of the compounds were determined in a final volume of 50 μl of reaction mixture consisting of 20 mM Tris-HCl, pH 7.5, 5 mM $MgCl_2$, 0.5 mM $MnCl_2$, 1 mM dithiothreitol, 50 mM NaCl, 400 ng of purified NS5B enzyme, 500 ng of poly(rA)·oligo$(dT)_{15}$ (Invitrogen), 30 μM UTP, and 1.5 μCi of α-^{32}P-labeled UTP (3000 Ci/mmol; Amersham Biosciences). RNA-dependent RNA polymerase reactions were allowed to proceed for 120 min. at 22 °C. The reactions were stopped by the addition of 10 μl of 0.5 mM EDTA. Thereafter, a volume of 50 μl (25 μg) of salmon sperm DNA (Invitrogen) and 100 μl of a solution of 20% trichloroacetic acid at 4 °C were added to the mixture followed by incubation on ice for 30 min to ensure complete precipitation of nucleic acids. The samples were then transferred onto 96-well MultiScreen filter plates (Millipore). The filter plates were washed with 600 μl of 1% trichloroacetic acid per well and dried for 20 min at 37 °C. 50-μl of liquid scintillation mixture (Wallac Oy, Turku, Finland) was added, and the incorporated radioactivity was quantified using a liquid scintillation counter (Wallac MicroBeta Trilux; PerkinElmer Life Sciences). The IC_{50} values were calculated using the computer software GraphPad Prism (version 2.0; GraphPad Software Inc., San Diego, CA).

Crystallization and Data Collection—Crystals of HCV 2a NS5B were grown by the hanging drop method at room temperature. 3 μl of reservoir solution (15% polyethylene glycol 8000, 0.2 M ammonium sulfate, 80 mM sodium citrate, pH 6.0, 7% glycerol, 4% 1,6-hexanediol, and 1% benzamidine) were mixed with 1.5 μl of protein solution (10 mg/ml protein concentration in 50 mM citrate buffer, pH 6.0, 5% glycerol, and 5 mM β-mercaptoethanol), and the resultant drops were equilibrated against 1 ml of reservoir solution. Needle-shaped crystals grew to a maximum size (0.04 × 0.04 × 0.5 mm) within 2–4 days. Two crystal forms of the enzyme were observed from different protein preparations. Both crystal forms belong to the space group $C222_1$ but differ markedly in the *a*-axis unit cell dimension (Table I). Throughout this paper the crystal form with the larger *a* cell dimension will be referred to as form I, whereas that with the smaller *a* cell dimension will be referred to as form II. Protein/inhibitor complexes were prepared by soaking experiments. Crystals were soaked in 2 mM inhibitor solution for ~12 h.

Intensity data from both crystal forms and from the protein-inhibitor B complex were collected at the beam line 8.3.1 of the Advanced Light Source in Berkeley, CA, whereas data from the protein-inhibitor A complex were collected using an R-AXIS IV ++ image plate detector with copper Kα radiation generated by a Rigaku RU-300 rotating anode x-ray generator. Both crystal forms contain one NS5B molecule in the asymmetric unit with solvent contents of ~64 and 60% in form I and form II, respectively (26). The data sets were indexed, integrated, and scaled using the programs DENZO and SCALEPACK (27). Data collection statistics of both crystal forms and the protein-inhibitor complexes are given in Table I.

Structure Determination and Refinement—Structure solutions of both crystal forms were achieved by molecular replacement with the CNS package (28) using the unliganded 1b genotype polymerase structure (8) (Protein Data Bank code 1C2P) as the search model. The inhibitor complex structures were solved by the difference Fourier method. A difference Fourier map, $|F_{PI}| - |F_P|$ (α_{calc} ($|F_{PI}|$ values of the protein-inhibitor complex and $|F_P|$ values from the apoprotein), permitted an initial positioning of the inhibitor molecule into the difference density. Structure refinement was carried out with the CNS package using a maximum likelihood target (28). All of the structures reported here were refined in the same manner. Initially, the structure was refined by treating the whole molecule as a rigid body. Subsequently, the model was subjected to iterations of positional refinement, simulated annealing, torsion angle dynamics, and individual *B*-factor refinement. Electron density maps ($2|F_o| - |F_c|$ and $|F_o| - |F_c|$) were calculated at this stage of refinement, and model building was performed wherever necessary using XtalView (29). Extensive model building was done in

TABLE I
Data collection and refinement statistics

Crystal	Form I	Form II	Complex A	Complex B
Space group	$C222_1$	$C222_1$	$C222_1$	$C222_1$
a (Å)	64.40	60.76	60.58	61.11
b (Å)	214.42	215.04	214.62	214.82
c (Å)	123.19	124.14	124.04	124.41
Z	8	8	8	8
Unit cell volume (Å^3)	1,701,091.2	1,608,262.4	1,612,771.4	1,633,210.9
Solvent content (%)	63.4	61.3	61.4	61.8
Data collection				
Temperature (K)	100	100	100	100
Detector	ADSC Q210	ADSC Q210	R-AXIS IV	ADSC Q210
Wavelength (Å)	1.100028	1.115870	1.54178	1.100028
Resolution (Å)	40–1.9	40–2.5	40–2.2	40 - 2.0
High resolution (Å)	1.97–1.9	2.59–2.5	2.28–2.2	2.07–2.0
Total observations	216176	98070	121520	197022
Unique reflections	65,644 (5,343)	27,506 (2,607)	40,067 (3,702)	55,391 (5,383)
Multiplicity	3.3 (2.5)	3.6 (3.4)	3.0 (2.5)	3.5 (3.3)
$I/\sigma(I)$[a]	12.7 (1.7)	9.4 (2.9)	6.7 (2.2)	9.8 (1.8)
Completeness (%)	97.2 (90.3)	96.9 (97.8)	96.4 (90.3)	99.3 (97.3)
R_{sym} (%)[b]	6.5 (48.6)	13.8 (54.5)	11.8 (42.6)	7.9 (49.6)
Refinement				
Refinement resolution (Å)	40–1.9	40–2.5	40–2.2	40–2.0
Unique reflections (working/test)	62,315/3,329	26,159/1,347	38,061/2,006	52,589/2,802
R_{work}/R_{free}[c]	21.4/23.8	20.1/25.2	21.5/23.4	20.8/24.4
Number of residues	1–563[d]	1–548	1–548	1–548
Number of water molecules	434	339	348	471
Mean *B*-factor (Å^2)[e]	26.5/-/35.5	27.8/-/30.2	33.1/29.2/37.4	34.2/25.5/41.1
Root mean square deviations from ideality				
Bond lengths (Å)	0.005	0.006	0.006	0.005
Bond angle (°)	1.2	1.3	1.3	1.3
Dihedral angles (°)	21.7	21.7	21.6	21.4
Improper angles (°)	0.80	0.83	0.81	0.84
Percentage of residues in Ramachandran plot				
In most favored regions (%)	91.0	88.8	89.7	90.3
In additional allowed regions (%)	8.6	10.6	9.9	9.7

[a] Value in parentheses refers to the high resolution shell.
[b] $R_{sym} = \Sigma_h\Sigma_i(|I_i(h) - \langle I(h)\rangle|)/\Sigma_h\Sigma_i I_i(h)$, where $I_i(h)$ is the *i*th intensity measurement and $\langle I(h)\rangle$ is the weighted mean of all measurements of $I(h)$.
[c] R_{work} and $R_{free} = \Sigma_h(|F(h)_{obs}| - |F(h)_{calc}|)/\Sigma_h|F(h)_{obs}|$ for reflections in the working and test sets (5% of data).
[d] Except for residues 149–153.
[e] Average *B*-factors for protein atoms, inhibitor atoms, and water molecules, respectively. Dash indicates no data.

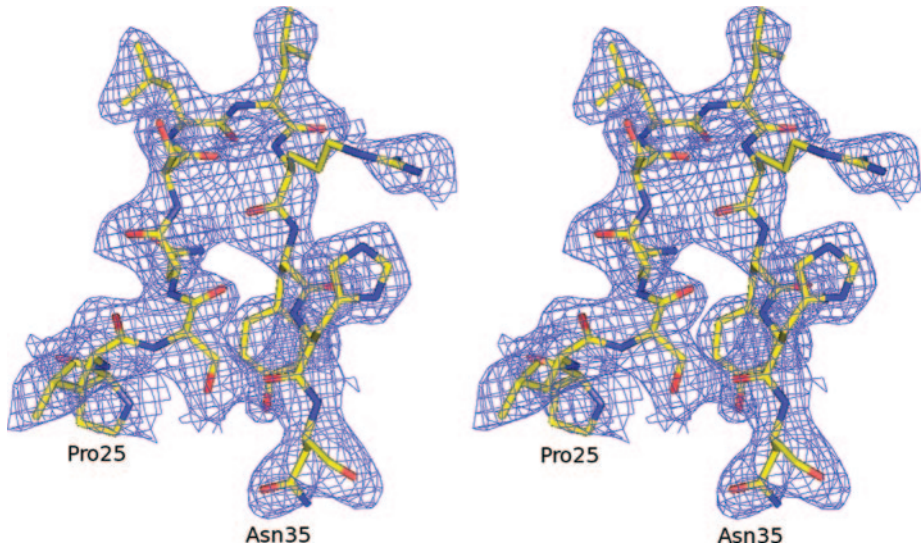

FIG. 2. **Stereo view of $2|F_o| - |F_c|$ electron density map contoured at the 1 σ level of the region Pro^{25}–Asn^{35} of the molecule in form II crystals.** Carbon, nitrogen, and oxygen atoms are represented in *gold*, *blue*, and *red*, respectively.

the thumb domain of the molecule in form II. The refinement was continued using CNS. The R_{work} and R_{free} values were monitored closely throughout the refinement. Once the refinement had converged to an R_{work} value of 0.24, identification of bound water molecules in the model was carried out. This was achieved in several stages based on electron density peaks of at least 3 σ in $|F_o| - |F_c|$ and 1 σ in $2|F_o| - |F_c|$ maps. Cycles of position and *B*-factor refinement, correction of the model using Fourier maps, and the identification of water molecules continued until no significant peaks were left in the electron density maps. Bulk solvent correction and anisotropic *B*-factor scaling were incorporated during the entire refinement. The molecule in form I was well defined in the electron density maps except for the region Pro^{149}–Gly^{153}. The electron density maps for the form II crystals were very clear for all the residues from Ser^1 to Lys^{548}. The electron density map corresponding to a portion of the Δ1 loop, Pro^{25}–Asn^{35} of the form II crystals is shown in Fig. 2. The stereochemical validity of the structure was examined using PROCHECK (30). In all of the structures >88% of the total number of residues lie in the most allowed regions of the Ramachandran plot. The refinement parameters are given in Table I. The refined atomic coordinates have been deposited in the Protein Data Bank (accession codes 1YUY, 1YV2, 1YVZ, and 1YVX for the form I, form II, and the NS5B-inhibitors A and B complexes, respectively).

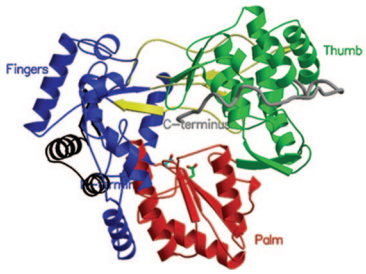

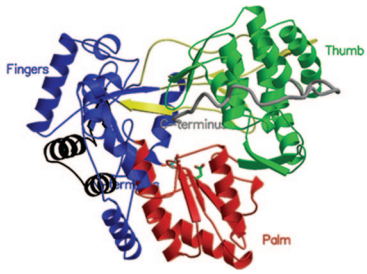

FIG. 3. **Stereo view of the overall structure of HCV polymerase genotype 2a in crystal form II.** *Blue*, *red*, and *green* colors correspond to the fingers, palm, and thumb domains, respectively. The two loops protruding from the fingers domain are indicated in *yellow*. Two antiparallel helices connecting the fingers and palm domains are shown in *black*. Two active site aspartates are shown by *stick* representation. The figure was prepared using the program MOLSCRIPT (31).

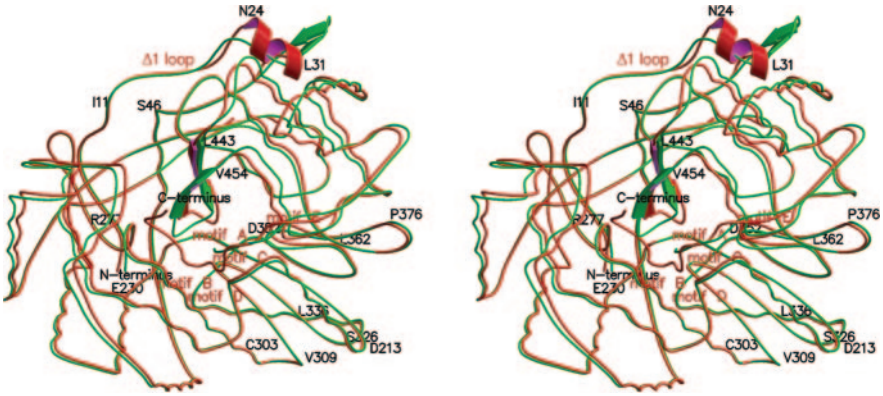

FIG. 4. **Coil representation of molecules in both crystal forms, showing the differences between the Δ1 loop (Ile^{11}–Ser^{46}) and the β-flap region (Leu^{443}–Val^{454}).** *Red* color represents the molecule in form I, whereas the molecule in form II is shown in *green*. Single letter amino acid abbreviations are used with position numbers.

RESULTS AND DISCUSSION

Overall Features of NS5B Polymerase in Form I and Form II—The three-dimensional structures of the NS5B HCV polymerase genotype 2a in both crystal forms have the same right-hand disposition of fingers, palm, and thumb domains (Fig. 3) as seen in HCV polymerase genotype 1b and also in other polymerases. However, the detailed structure of the polymerase in form I is substantially different from that in form II. The loop (Δ1) protruding from the fingers domain and comprising residues Ile^{11}–Ser^{46} (Fig. 4) exhibits significant structural variability in both forms. The root mean square deviation of a part (Lys^{20}-Thr^{40}) of this loop between the two molecules is 1.82 Å (16 Cα atoms) as compared with the overall root mean square deviation of 1.08 Å (531 Cα atoms). The region Asn^{24}–Leu^{31} is a helix in form I, whereas in form II it is part of a small β-hairpin (Fig. 4). The average *B*-factor of the protein atoms of NS5B molecule in form II is 27.8 Å^2, whereas the average *B*-factor of the atoms of the Lys^{20}–Thr^{40} residues is 47.7 Å^2, indicating a high degree of flexibility in this region. The molecule in form I is relatively rigid, as is evident from its relatively low *B*-factors. The average *B*-factors are 26.5 and 30.0 Å^2 for protein atoms of the entire molecule and atoms in the region Lys^{20}–Thr^{40}, respectively. Extensive interactions between the extension (Δ1 loop) from the fingers domain and the thumb domain of the molecule in form I maintain the polymerase in a more rigid arrangement. The number of van der Waals interactions at the fingers-thumb domains interface listed in Table II shows that the molecule in form I has 28% more intramolecular interactions than the molecule in form II. The hydrogen bonding networks in the region Lys^{20}–Thr^{40} are listed in Table III, and the observed differences clearly demonstrate that the molecules adopt different secondary structures in this region. An analysis of the crystal packing interactions indicates that the neighboring molecules in the crystal lattice have very little effect on the conformation of the region Lys^{20}–Thr^{40} in both crystal forms. Recent studies on HCV polymerase genotype 1b involving the mutation of Leu^{30} to polar serine or arginine amino acids resulted in a non-functional polymerase, presumably due to a local perturbation in the Δ1 loop (32). Our studies therefore provide structural evidence that the Δ1 loop is, to a major extent, responsible for determining the active state of HCV polymerase genotype 2a and, by analogy, for other RNA polymerases including the polymerase of HCV genotype 1b.

TABLE II

List of residues making van der Waals contacts (distance cut-off 4 Å) between the extension from the fingers (Δ1 loop) and thumb domains of the molecules in crystal forms I and II

The number of contacts between the residues are given in parentheses.

Form I	Form II
Glu^{18}–Trp^{397} (4)	Glu^{18}–Trp^{397} (3)
Glu^{18}–Arg^{401} (8)	Glu^{18}–Arg^{401} (11)
Lys^{20}–Trp^{397} (4)	Leu^{21}–Trp^{397} (10)
Leu^{21}–Trp^{397} (6)	Leu^{21}–Arg^{401} (1)
Pro^{22}–Val^{400} (1)	Pro^{22}–Arg^{401} (1)
Pro^{22}–Arg^{401} (4)	Ile^{23}–Val^{400} (1)
Asn^{24}–Val^{400} (3)	Asn^{24}–Ala^{396} (3)
Leu^{26}–Thr^{399} (1)	Pro^{25}–Thr^{399} (1)
Leu^{26}–His^{428} (1)	Pro^{25}–Val^{400} (2)
Ser^{27}–Ala^{396} (3)	Pro^{25}–His^{428} (1)
Ser^{27}–Val^{400} (2)	Leu^{26}–Ala^{396} (4)
Ser^{29}–Pro^{495} (2)	Leu^{26}–His^{428} (5)
Ser^{29}–Trp^{500} (2)	Leu^{26}–Ala^{494} (1)
Ser^{29}–Arg^{503} (4)	Leu^{26}–Pro^{495} (1)
Leu^{30}–Ile^{392} (1)	Leu^{26}–Trp^{500} (2)
Leu^{30}–Ala^{396} (3)	Ser^{27}–Leu^{492} (1)
Leu^{30}–Val^{424} (1)	Ser^{27}–Gly^{493} (5)
Leu^{30}–His^{428} (3)	Ser^{27}–Ala^{494} (1)
Leu^{30}–Ala^{494} (2)	Asn^{28}–Arg^{503} (1)
Leu^{30}–Pro^{495} (1)	His^{34}–Gly^{493} (4)
Leu^{30}–Trp^{500} (2)	Lys^{36}–Lys^{491} (4)
Leu^{31}–Ala^{396} (1)	Lys^{36}–Leu^{492} (2)
Leu^{31}–Leu^{492} (4)	Val^{37}–Ala^{393} (4)
Leu^{31}–Gly^{493} (2)	Val^{37}–Trp^{397} (1)
Leu^{31}–Ala^{494} (1)	Cys^{39}–Trp^{397} (2)
Arg^{32}–Leu^{492} (1)	
Arg^{32}–Gly^{493} (7)	
Tyr^{33}–Arg^{490} (1)	
Tyr^{33}–Lys^{491} (2)	
Tyr^{33}–Leu^{492} (8)	
Tyr^{33}–Gly^{493} (7)	
Lys^{36}–Lys^{491} (4)	
Cys^{39}–Trp^{397} (3)	

TABLE III
Comparison of hydrogen bondings between molecules in form I and form II at the fingers and thumb domains interface

Molecule in form I (MM[a])		Molecule in form II (MM[a])		Molecule in form I (MS,[b] SM,[c] SS[d])		Molecule in form II (MS,[b] SM,[c] SS[d])	
Donor	Acceptor	Donor	Acceptor	Donor	Acceptor	Donor	Acceptor
Leu^{21} N	Val^{37} O			Leu^{26} N	Asn^{24} OD2		
Asn^{28} N	Asn^{24} O			Ser^{29} OG	Leu^{26} O		
Ser^{29} N	Pro^{25} O			Arg^{503} NH2	Ser^{29} O		
Leu^{30} N	Ser^{27} O			Arg^{32} NE	Gly^{493} O		
Leu^{31} N	Ser^{27} O			His^{34} ND1	Arg^{32} O		
Arg^{32} N	Gly^{493} O			Lys^{36} NZ	Lys^{491} O		
His^{34} N	Arg^{32} O			Lys^{155} N	Tyr^{38} OH	Lys^{155} N	Tyr^{38} OH
Val^{37} N	His^{34} O			Thr^{40} OG1	Lys^{141} O	Thr^{40} OG1	Lys^{141} O
		Ser^{29} N	Arg^{32} O	Glu^{143} N	Thr^{40} OG1	Glu^{143} N	Thr^{40} OG1
		Arg^{32} N	Ser^{29} O	Thr^{40} OG1	Glu^{143} O	Thr^{40} OG1	Glu^{143} O
		His^{34} N	Ser^{27} O				
						Asn^{35} ND2	Leu^{21} O
Val^{147} N	Lys^{36} O	Val^{147} N	Lys^{36} O			Asn^{24} N	Tyr^{33} OH
Tyr^{38} N	Phe^{145} O	Tyr^{38} N	Phe^{145} O			Ser^{27} N	Asn^{24} OD1
Phe^{145}N	Tyr^{38} O	Phe^{145}N	Tyr^{38} O			Asn^{24} ND2	Asn^{35} OD1
Thr^{40} N	Glu^{143} O	Thr^{40} N	Glu^{143} O			Ser^{27} OG	His^{34} O
						Arg^{503} NH1	Asn^{28} O

[a] MM, main chain-main chain.
[b] MS, main chain-side chain.
[c] SM, side chain-main chain.
[d] SS, side chain-side chain.

TABLE IV
Structures used in the analysis

Structure 1, HCV polymerase genotype 1b Δ 21 (8); structure 2, HCV polymerase genotype 1b Δ 55 (9); structure 3, HCV polymerase genotype 1b Δ 21 (10); structure 4, HCV polymerase genotype 1b HC-J4 Δ 21 (12); structure 5, HCV polymerase genotype 2a, form I; structure 6, HCV polymerase genotype 2a, form II; structure 7, HCV polymerase genotype 2a complexed with inhibitor A; structure 8, HCV polymerase genotype 2a complexed with inhibitor B.

Structure	Space group	Resolution (Å)	PDB code	Average *B*-factor of protein atoms	Solvent-accessible Surface area
				Å²	*Å²*
1	$P2_12_12_1$	1.9	1C2P	48.4	23873
2	$P2_12_12_1$	2.8	1CSJ	31.0	23407
3	$P4_32_12$	2.5	1QUV	27.9	23868
4	$P2_12_12_1$	2.0	1NB4	43.5	24672
5	$C222_1$	1.9	1YUY	26.5	23477
6	$C222_1$	2.5	1YV2	27.8	24955
7	$C222_1$	2.2	1YVZ	33.1	24657
8	$C222_1$	2.0	1YVX	34.2	24765

Between the form I and form II, the fingers domain also undergoes noticeable structural changes as each Cα atom in the region Ala^{80}–Lys^{120} moves by >1 Å. Superimpositions were done using the program Align (33). The palm domain (residues Gly^{188}–Asp^{225} and Thr^{287}–Val^{370}), which includes catalytic residues (Asp^{220} and Asp318), maintains the same geometry in both molecules. The root mean square deviation of the palm domain between the two molecular forms is 0.26 Å. The conformations of the structural motifs A–E (motif A, residues Asp^{213}–Glu^{230}; motif B, residues Arg^{277}–Cys^{303}; motif C, residues Val^{309}–Ser^{326}; motif D, residues Leu^{336}–Asp^{352}; and motif E, residues Leu^{362}–Pro^{376}) remain essentially the same between these two molecules.

The largest structural changes that are observed are in the thumb domain; the main difference between form I and form II is a rigid body rotation of 7.5° of the thumb domain relative to the fingers and palm domains. It is known that the thumb domain moves during the formation of the ternary complex in human immunodeficiency virus type 1 reverse transcriptase (17) and also between the two independent molecules in the asymmetric unit, representing closed and open conformations of the RNA-dependent RNA polymerase of the rabbit hemorrhagic virus (15). In addition, a part of the thumb domain comprising residues Leu^{443}–Val^{454}, the β-flap region, moves as shown in Fig. 4. This region has been proposed to move and/or interact with RNA during elongation (8–10). This finding demonstrates that HCV polymerase genotype 2a can have an ensemble of conformations. The solvent-accessible surface area of the molecule in form II (Table IV) is 6% greater than that in form I, which further suggests that the molecule in form II is relatively open.

On the basis of the observed conformational variability in the thumb domain, the interface between the fingers and thumb domains, and the changes in the β-flap region, we provide structural evidence of the existence of closed and open conformations of the NS5B HCV polymerase genotype 2a. The molecule in crystal form I is in the closed (active) conformation, and that in crystal form II is in the open (inactive) conformation. This is the first structural evidence of the existence of an open conformation of NS5B HCV polymerase genotype 2a. More importantly, the conformations of the NS5B-inhibitor-bound structures, described later, resemble the conformation of the molecule in crystal form II. Hence, this finding would indicate that the molecule in crystal form II likely resembles the inactive conformation of the polymerase, although the conformation of catalytic aspartic residues in both forms remains the same.

Comparison of HCV NS5B Polymerases of Genotypes 2a and 1b—To date, crystal structure studies of HCV polymerase genotype 1b have revealed the molecular structure in several crystal forms (8–10). The structure determination of the HCV polymerase of genotype 1b led to the understanding of the overall three-dimensional structure of the enzyme and the architecture of its active site. Unlike other polymerase structures

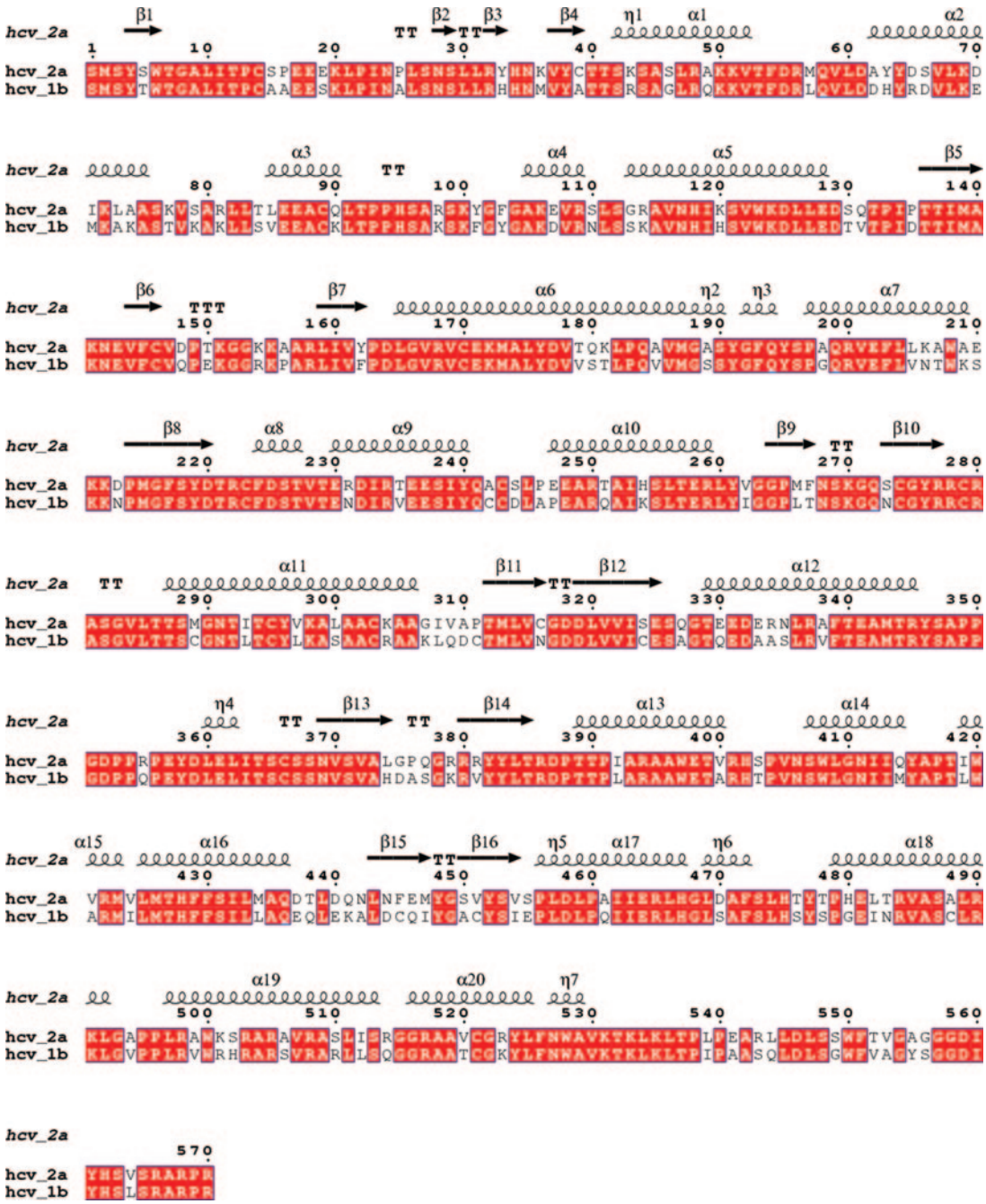

FIG. 5. **Comparison of sequences between HCV polymerase genotypes 1b and 2a.** Identical residues are shown in the *red boxes*. Also shown are the secondary structural elements corresponding to the structure of genotype 2a in form II. The figure was generated by the program ESPript (34).

TABLE V

Root mean square deviations (r.m.s.d.) between domains

The entries are r.m.s.d. between thumb domains (residues 371–529; 159 Cα atoms), palm domains (188–226 and 287–370; 123 Cα atoms), and fingers (1–10, 46–139, 161–187, 227–230 and 263–286; 160 Cα atoms) domains respectively. The values in the parentheses correspond to the r.m.s.d. between the pair of molecules. Only CA atoms were taken for r.m.s.d. calculation. The numbering of the structures is same as that in Table IV.

	2	3	4	5	6	7	8
1	0.85, 0.60, 0.69 (0.72)	0.82, 0.63, 0.75 (0.75)	0.48, 0.29, 0.43 (0.46)	0.58, 0.46, 0.54 (0.54)	1.68, 0.56, 0.88 (1.22)	1.55, 0.52, 0.89 (1.15)	1.62, 0.71, 0.83 (1.17)
2		1.27, 0.70, 0.85 (0.99)	1.17, 0.68, 0.79 (0.91)	0.77, 0.22, 0.62 (0.64)	1.09, 0.39, 0.71 (0.81)	0.98, 0.35, 0.67 (0.74)	0.98, 0.55, 0.65 (0.74)
3			0.64, 0.57, 0.59 (0.60)	0.85, 0.60, 0.89 (0.84)	1.61, 0.65, 0.85 (1.16)	1.47, 0.63, 0.84 (1.09)	1.21, 0.63, 0.75 (1.13)
4				0.76, 0.49, 0.62 (0.66)	1.66, 0.58, 0.83 (1.20)	1.56, 0.58, 0.84 (1.18)	1.59, 0.77, 0.76 (1.16)
5					1.24, 0.26, 0.98 (1.08)	1.36, 0.33, 0.97 (1.03)	1.34, 0.46, 0.98 (1.04)
6						0.27, 0.23, 0.22 (0.22)	0.29, 0.21, 0.15 (0.23)
7							0.17, 0.15, 0.10 (0.14)

determined by x-ray diffraction methods, the active site of HCV NS5B polymerase genotype 1b is completely encircled (8). Although the overall structure of the HCV polymerase genotype 2a from both crystal forms is similar to the structure of HCV polymerase genotype 1b, consistent with the high amino acids sequence identity of 75% (Fig. 5) over the entire polypeptide

chain, there are marked structural differences between the structures of the polymerases from these two genotypes. To understand the three-dimensional structure of HCV polymerase and its variability among different genotypes or in the same genotype in a different crystal environment, we have analyzed the available structures as listed in Table IV.

To elucidate the structural differences, the Cα atoms of pairs of molecules were superimposed. The resulting root mean square deviations are listed in Table V. From these results, it is apparent that, the structure of polymerase of genotype 2a in form I crystal is similar to the HCV polymerase genotype 1b structures. However, the molecule in crystal form II shows greater variation from other 1b polymerase structures and also from the molecule in crystal form I. Among the three domains, the thumb domain exhibits the greatest variation. The fingers domain, however, agrees much better. The palm domain preserves a relatively rigid structure across all of the molecules.

Effect of Non-nucleoside Inhibitors on NS5B Activity—Both thiophene 2-carboxylic acid inhibitors, namely compounds A and B (Fig. 1), were tested for anti-HCV polymerase genotype 2a activity using the C-terminal truncated form (Δ21) of the enzyme. Both compound A and B were found to be active against polymerase 2a in a dose-dependent manner with IC_{50} values of 4.4 and 8.0 μM, respectively (Fig. 6).

Inhibitor Binding Site and NS5B-Inhibitor Interaction—Thiophene-2-carboxylic acids A and B, found previously to be inhibitors of HCV polymerase genotype 1b, were also found to inhibit polymerase genotype 2a (Δ21 C-terminal truncated). Our observations from soaking experiments suggest that both inhibitors can only bind to crystal form I, because they cannot be soaked into the enzyme that crystallizes in form II. Unexpectedly, our analysis of the inhibitor/polymerase complex revealed that the enzyme has now adopted the form II crystal form (Table I). Based upon our crystallization experiments, for a given batch of protein purification only one of the two crystal forms can be obtained. Relatively few form I crystals were seen, whereas form II produced a large number of needle-shaped crystals.

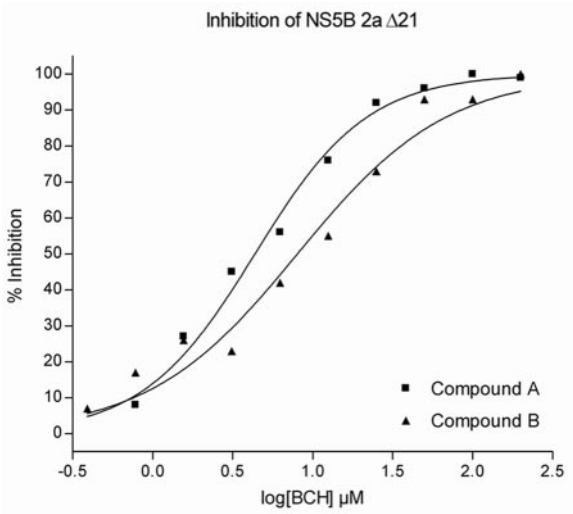

FIG. 6. **HCV NS5B genotype 2a activity as a function of compound A and compound B concentrations.**

As in other known polymerases, the HCV NS5B polymerase active site is situated in the palm domain. Two conserved aspartic acid residues (Asp^{220} and Asp^{318}) located in the palm domain along with two Mg^{2+} ions are essential for the polymerization reaction. Both inhibitors bind NS5B molecule in a shallow cavity on thumb domain (Fig. 7), and the inhibitor binding site is ~35 Å away from the polymerase active site. The simulated annealing omit electron density maps clearly revealed the orientation and conformation of all substituents of both inhibitors (Fig. 8, *a* and *b*). The NS5B-inhibitor interactions are very similar in both complex structures. The inhibitor binding site is primarily hydrophobic in nature. Amino acid residues Ile^{419}, Arg^{422}, Met^{423}, Leu^{474}, His^{475}, Thr^{476}, Tyr^{477}, Leu^{482}, Leu^{497}, Arg^{498}, Lys^{501}, and Trp^{528} form the binding pocket of the inhibitor. The 2,4-dichlorobenzoyl group of inhibitor A and the 4-methylbenzoyl group of inhibitor B are involved in extensive van der Waals interactions with residues Arg^{422}, Met^{423}, Leu^{474}, His^{475}, Tyr^{477}, Lys^{501}, and Trp^{528}. The isopropyl amino groups of both inhibitors do not interact with NS5B molecule, whereas the phenylthiophene moiety of both inhibitors are involved in van der Waals interactions with residues Ile^{419}, Leu^{482}, Leu^{497}, and Arg^{498}. The carboxyl oxygen atoms of the inhibitors are hydrogen-bonded to the main chain amide nitrogen atoms of residues Thr^{476} and Tyr^{477}. NS5B-inhibitor interactions are depicted in Fig. 9, *a* and *b*.

In an attempt to provide a rationale as to why the NS5B molecule in form II does not allow inhibitor complex formation, the inhibitors were docked to the form II molecular structures, and we observed that the generated NS5B-inhibitor interactions were virtually identical to the one obtained experimentally with form I NS5B. The only visible difference was the length of the hydrogen-bonding distance between the two carboxylate oxygen atoms of the inhibitor and the backbone amide nitrogens of the residues Thr^{476} and Tyr^{477}. The hydrogen bonding distance between the inhibitor's carboxylate O22 atom and the main chain amide nitrogen atom of residue Thr^{476} is 2.7 Å in the inhibitor bound structure, whereas in the inhibitor-docked structure the corresponding distance is 2.2 Å. A similar situation was observed for the other hydrogen bond between the inhibitor's carboxylate O21 atom and Tyr^{477}. It is therefore possible that the increased steric hindrance precludes inhibitors from binding. The other possibility could be that as the thumb domain of the molecule in form II moves by 7.5° with respect to the thumb domain of the molecule in form I, the conformation of the former may not be conducive for the inhibitors to be bound.

Conformational Changes upon Inhibitor Binding and Plausible Mechanisms of Inhibition—As mentioned earlier, only the NS5B polymerase in the closed conformation (form I), which is similar to that of the polymerase of genotype 1b conformation, binds the inhibitor. Upon inhibitor binding, NS5B undergoes major conformational changes as shown in Fig. 10. Three regions of the molecule undergo major structural changes. The

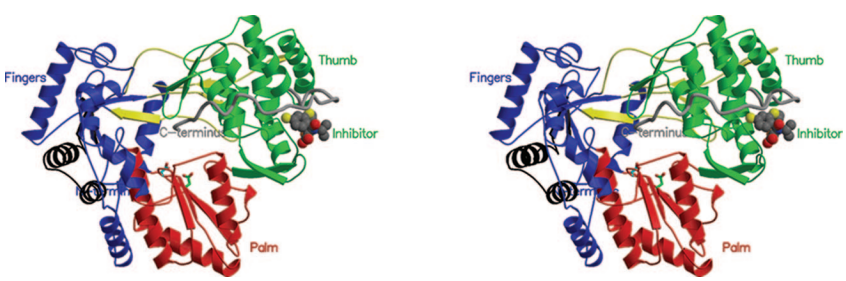

FIG. 7. **Illustration of the binding site of the inhibitors.** Because both inhibitors bind at the same site located in the thumb domain, only inhibitor A is shown in a Corey, Pauling, Koltun (CPK) space-filling model with carbon atoms in *gray*. Other color codes are same as those describe in the Fig. 3 legend.

thumb domain moves ~7.5° relative to the fingers and palm domains, the fingers-thumb domains interface, and the β-flap region. The nature of the conformational changes resulting upon inhibitor binding is similar for both inhibitors (Fig. 10). The inhibitor-bound structures of NS5B are very similar to the unbound structure of NS5B molecule in form II. As presented in Table III, the average *B*-factors of the protein atoms of the inhibitor-bound structures are larger than those of the native structures, indicating that, the former structures are relatively flexible.

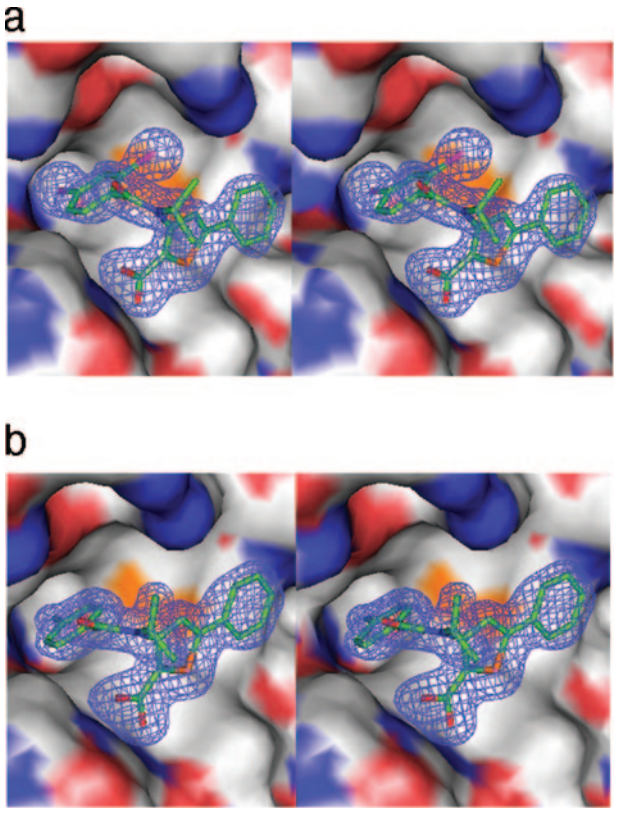

FIG. 8. **Stereo views of simulated annealed omit $|F_o| - |F_c|$ electron density maps contoured at the 3 σ level for the inhibitor A complex (*a*) and the inhibitor B complex (*b*).** The final refined inhibitor models are superimposed on the electron density maps. Inhibitors are shown as *stick* models with carbon, nitrogen, oxygen, sulfur, and chloride atoms in *green*, *blue*, *red*, *orange*, and *magenta*, respectively. The inhibitor-binding site is shown by surface representation with carbon, nitrogen, and oxygen in *gray*, *blue*, and *red*, respectively. The figure was prepared by the program PyMol (pymol.sourceforge.net) (35).

On the basis of the major conformational changes in the NS5B molecule observed upon inhibitor binding, we propose the following mechanisms of inhibition. Upon inhibitor binding, the Δ1 loop, an extension from the fingers domain, moves away from the thumb domain to reduce the inter-fingers-thumb domain interactions, thereby resulting in a perturbation of the integrity of the structure. Part of the Δ1 loop (residues Asn^{24}-Leu^{31}), which adopts a helical conformation in the native structure (form I), changes to a small β-hairpin-like structure in the inhibitor-bound structures. It is therefore possible that inhibitor binding triggers the unwinding of this helix, thus inducing the 7.5° shift in the thumb domain relative to the fingers and palm domains. In the presence of an inhibitor, the polymerase is "locked" into form II and is incapable of polymerization or reverting back to the active form I. Recent studies on HCV polymerase genotype 1b have provided some insight into the importance of the Δ1 loop in coordinating the motion between the thumb and finger domains, hence giving rise to the "closed" or "open" conformation. Labonté *et al.* have shown by analytical ultracentrifugation experiments that substitution of Leu^{30} by polar serine or arginine results in a nonfunctional polymerase due to a local perturbation in the Δ1 loop that impairs the ability of the thumb domain to assume the closed conformation (32). Furthermore, this displacement of the Δ1 loop may also impair its ability to bind the allosteric modulator rGTP at the outer thumb region. The ability of the polymerase to oligomerize to the functional enzyme may also be prevented, as one of the key amino acids involved in that process (Glu^{18}) forms part of the Δ1 loop. Our studies therefore provide, in addition to the mode of action of the thiophene-2-carboxylic acid inhibitors, structural evidence that the Δ1 loop is indeed responsible for determining the active state of HCV polymerase genotype 2a and, by analogy, of other RNA-depend-

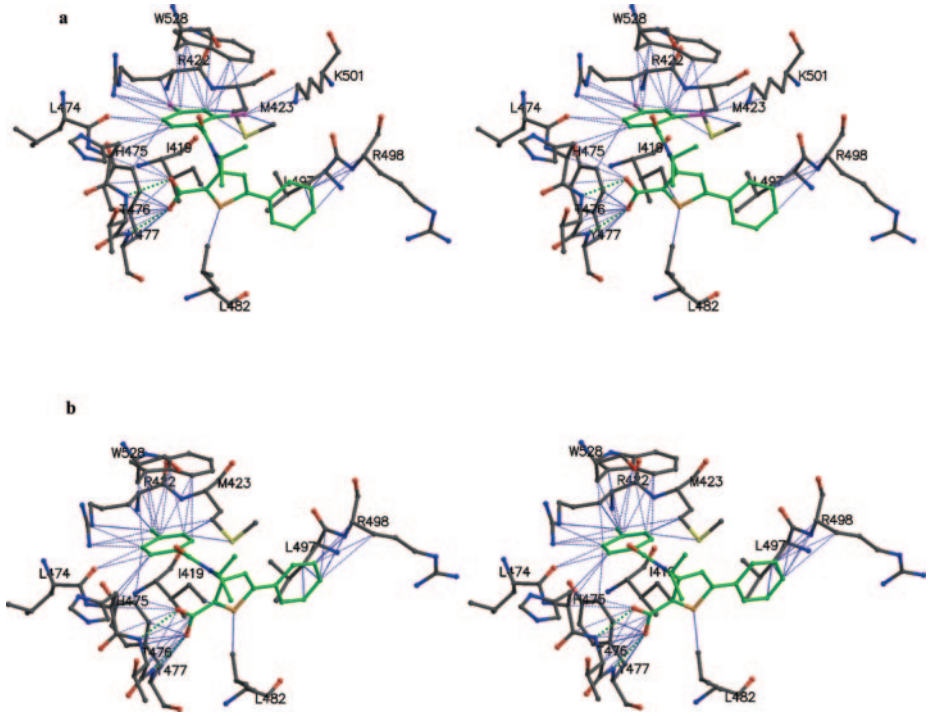

FIG. 9. **Stereo views of the NS5B polymerase-inhibitor A (*a*) and NS5B polymerase-inhibitor B (*b*) interactions.** The carbon, nitrogen, oxygen, and sulfur atoms of the protein are shown in *gray*, *blue*, *red*, and *yellow*, respectively. The color codes used to represent the inhibitors are same as those described in the Fig. 8 legend. Hydrogen bonding and van der Waals interactions are shown in *green* and *blue*, respectively. Single letter amino acid abbreviations are used with position numbers.

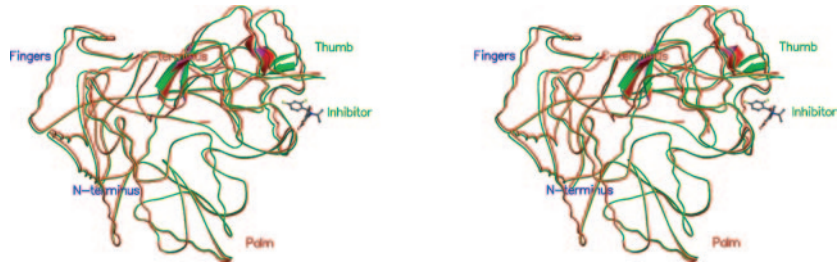

FIG. 10. **Stereo view of conformational changes that occur upon inhibitor binding.** Inhibitor bound and unbound structures are superimposed. Because similar conformational changes were observed in the case of both inhibitors, only that induced by inhibitor A is shown. *Green* and *red* colors correspond to the inhibitor bound and unbound structures, respectively.

ent RNA polymerases, including the polymerase of HCV genotype 1b. Although these experiments have provided structural evidence on the mechanism of action of the thiophen-2-caroxylic acid inhibitors, further investigations are needed to assess the influence of RNA templates, substrate nucleotides, and the allosteric rGTP on the inhibition mechanism.

Structure-based mutations of residue Leu^{30} to either serine or arginine reduces the activity of the polymerase (32). Hence, the Δ1 loop and thumb domain interface is critical for the polymerase activity. Perturbation of this region would ultimately affect the activity. Second, the substantial movement of the thumb domain (7.5°) relative to the fingers and palm domains upon inhibitor binding may inhibit the function of polymerase, as it is known that the thumb domain moves by a similar magnitude between the proposed active and inactive structures of the RNA-dependent RNA polymerase of rabbit hemorrhagic virus (15).

In summary, the structures of two crystal forms of HCV polymerase genotype 2a have been determined. These two forms correspond to a closed and an open conformation of the NS5B polymerase. Structure analysis has provided insights into our understanding of the structural variability among different genotypes and different crystal environments of the same genotype. Enzyme-inhibitor complexes could only be generated with the crystal form I, which is the closed form and is believed to be the active entity. The presence of the inhibitor was found to induce conformational changes that result in the open or inactive form.

Acknowledgment—We thank the Alberta Synchrotron Institute for data collection on beamline 8.3.1 at the Advanced Light Source, Berkeley, CA.

REFERENCES

1. Rice, C. M. (1996) in *Fields Virology* (Fields, B. N., Knipe, D. M., Howley, P. M., Chanock, R. M., Melnick, J. L., Monath, T. P., and Roizman, B., eds) Vol. 1, 3rd Ed., pp 931–959, Lippincott-Raven Press, Philadelphia
2. Bartenschlager, R. (1997) *Intervirology* **40,** 378–393
3. Kato, N., Hijikata, M., Ootsuyama, Y., Nakagawa, M., Ohkoshi, S., Sugimura, T., and Shimotohno, K. (1990) *Proc. Natl. Acad. Sci. U. S. A.* **87,** 9524–9528
4. Takamizawa, A., Mori, C., Fuke, I., Manabe, S., Murakami, S., Fujita, J., Onishi, E., Andoh, T., Yoshida, I., and Okayama, H. (1991) *J. Virol.* **65,** 1105–1113
5. Grakoui, A., Wychowski, C., Lin, C., Feinstone, S. M., and Rice, C. M. (1993) *J. Virol.* **67,** 1385–1395
6. Hagedorn, C. H., Van Beers, E. H., and De Staercke, C. (2000) *Curr. Top. Microbiol. Immunol.* **242,** 225–260
7. Lohmann, V., Korner, F., Herian, U., and Bartenschlager, R. (1997) *J. Virol.* **71,** 8416–8428
8. Lesburg, C. A., Cable, M. B., Ferrari, E., Hong, Z., Mannarino, A. F., and Weber, P. C. (1999) *Nat. Struct. Biol.* **6,** 937–943
9. Bressanelli, S., Tomei, L., Roussel, A., Incitti, I., Vitale, R. L., Mathieu, M., De Francesco, R., and Rey, F. A. (1999) *Proc. Natl. Acad. Sci. U. S. A.*, **96,** 13034–13039
10. Ago, H., Adachi, T., Yoshida, A., Yamamoto, M., Habuka, N., Yatsunami, K., and Miyano, M. (1999) *Structure Fold. Des.* **7,** 1417–1426
11. Bressanelli, S., Tomei, L., Rey, F. A., and De Francesco, R. (2002) *J. Virol.* **76,** 3482–3492
12. O'Farrell, D., Trowbridge, R., Rowlands, D., and Jager, J. (2003) *J. Mol. Biol.* **326,** 1025–1035
13. Hansen, J. L., Long, A. M., and Schultz, S. C. (1997) *Structure* **5,** 1109–1122
14. Butcher, S. J., Grimes, J. M., Makeyev, E. V., Bamford, D. H., and Stuart, D. I. (2001) *Nature*, **410,** 235–240
15. Ng, K. K., Cherney, M. M., Vazquez, A. L., Machin, V. A., Alonso, J. M., Parra, F., and James, M. N. (2002) *J. Biol. Chem.* **277,** 1381–1387
16. Rodgers, D. W., Gamblin, S. J., Harris, B. A., Ray, S., Culp, J. S., Hellmig, B., Woolf, D. J., Debouck, C., and Harrison, S. C. (1995) *Proc. Natl. Acad. Sci. U. S. A.* **92,** 1222–1226
17. Huang, H., Chopra, R., Verdine, G. L., and Harrison, S. C. (1998) *Science* **282,** 1669–1675
18. Lesburg, C. A., Radfar, R., and Weber, P. C. (2000) *Curr. Opin. Investig. Drugs* **1,** 289–296
19. Love, R. A., Parge, H. E., Yu, X., Hickey, M. J., Diehl, W., Gao, J., Wriggers, H., Ekker, A., Wang, L., Thomson, J. A., Dragovich, P. S., and Fuhrman, S. A. (2003) *J. Virol.* **77,** 7575–7581
20. Wang M., Ng, K. K., Cherney, M. M., Chan, L., Yannopoulos, C. G., Bedard, J., Morin, N., Nguyen-Ba, N., Alaoui-Ismaili, M. H., Bethell, R. C., and James, M. N. (2003) *J. Biol. Chem.* **278,** 9489–9495
21. Chan, L., Reddy, T. J., Proulx, M., Das, S. K., Pereira, O., Wang, W., Siddiqui, A., Yannopoulos, C. G., Poisson, C., Turcotte, N., Drouin, A., Alaoui-Ismaili, M. H., Bethell, R., Hamel, M., L'Heureux, L., Bilimoria, D., and Nguyen-Ba, N. (2003) *J. Med. Chem.* **46,** 1283–1285
22. Chan, L., Das, S. K., Reddy, T. J., Poisson, C., Proulx, M., Pereira, O., Courchesne, M., Roy, C., Wang, W., Siddiqui, A., Yannopoulos, C. G., Nguyen-Ba, N., Labrecque, D., Bethell, R., Hamel, M., Courtemanche-Asselin, P., L'Heureux, L., David, M., Nicolas, O., Brunette, S., Bilimoria, D., and Bedard, J. (2004) *Bioorg. Med. Chem. Lett.* **14,** 793–796
23. Chan, L., Pereira, O., Reddy, T. J., Das, S. K., Poisson, C., Courchesne, M., Proulx, M., Siddiqui, A., Yannopoulos, C. G., Nguyen-Ba, N., Roy, C., Nasturica, D., Moinet, C., Bethell, R., Hamel, M., L'Heureux, L., David, M., Nicolas, O., Courtemanche-Asselin, P., Brunette, S., Bilimoria, D., and Bedard, J. (2004) *Bioorg. Med. Chem. Lett.* **14,** 797–800
24. Stemmer, W. P., Crameri, A., Ha, K. D., Brennan, T. M., and Heyneker, H. L. (1995) *Gene* **164,** 49–53
25. Alaoui-lsmaili, M. H., Hamel, M., L'Heureux, L., Nicolas, O., Bilimoria, D., Labonte, P., Mounir, S., and Rando, R. F. (2000) *J. Hum. Virol.* **3,** 306–316
26. Matthews, B. W. (1968) *J. Mol. Biol.* **33,** 491–497
27. Otwinowski, Z., and Minor, W. (1997) *Methods Enzymol.* **276,** 307–326
28. Brunger, A. T., Adams, P. D., Clore, G. M., DeLano, W. L., Gros, P., Grosse-Kunstleve, R. W., Jiang, J. S., Kuszewski, J., Nilges, M., Pannu, N. S., Read, R. J., Rice, L. M., Simonson, T., and Warren, G. L. (1998) *Acta Crystallogr. Sect. D Biol. Crystallogr.* **54,** 905–921
29. McRee, D. E. (1999) *J. Struct. Biol.* **125,** 156–165
30. Laskowski, R. A., MacArthur, M. W., Moss, D. S., and Thornton, J. M. (1993) *J. Appl. Crystallogr.* **26,** 283–291
31. Kraulis, P. J. (1991) *J. Appl. Crystallogr.* **24,** 946–950
32. Labonté, P., Axelrod, V., Agarwal, A., Aulabaugh, A., Amin, A., and Mak, P. (2002) *J. Biol. Chem.* **277,** 38838–38846
33. Cohen, G. H. (1997) *J. Appl. Crystallogr.* **30,** 1160–1161
34. Gouet, P., Courcelle, E., Stuart, D. I., and Metoz, F. (1999) *Bioinformatics* **15,** 305–308
35. DeLano, W. L. (2002) *The PyMOL User's Manual*, DeLano Scientific, San Carlos, CA